CrystEngComm

ROYAL SOCIETY OF CHEMISTRY

PAPER

View Article Online
View Journal | View Issue

Cite this: *CrystEngComm*, 2024, **26**, 6361

Exploring the host–guest interactions of small molecules in UoC-9(Ca)†

Sean S. Sebastian, Finn P. Dicke and Uwe Ruschewitz *

The Ca-based fluorinated MOF, named UoC-9 (UoC = University of Cologne), was previously published, crystallising in an orthorhombic crystal system with a 2nd order phase transition (*Ima*2 to *Pna*2_1) between room temperature and 100 K. Herein, this MOF was used as a crystalline sponge to embed a selection of six different small guest molecules inside its pores by liquid exchange. After confirming that the guest molecules were successfully loaded into the pores of UoC-9, the resulting host–guest systems were extensively analysed *via* single crystal X-ray diffraction. The different crystal structures allowed us to investigate the structural behaviour of UoC-9 in response to the embedded guest molecules. The lattice parameters as well as the phase transition are influenced differently by the various guests, which is described in detail by supplementary Hirshfeld surface analyses enabling us to examine the underlying host–guest interactions. The NMP@UoC-9 (NMP = *N*-methyl-2-pyrrolidone) system exhibits superstructure reflections with a tripled *b*-axis, which was also elucidated within this work.

Received 3rd October 2024,
Accepted 23rd October 2024

DOI: 10.1039/d4ce01007h

rsc.li/crystengcomm

Introduction

Over the last three decades, metal–organic frameworks (MOFs) have undergone an incredible development from the first mention of the term in 1995 (ref. 1) to their research for a wide range of potential applications.[2–4] The porosity of MOFs, along with the ability to control and tune many of its properties *via* chemical modification, is one of the major aspects that makes these materials so attractive to chemists.[5] Modifying the internal surface of MOFs by functionalization of the organic linkers, has led to vast improvements of a variety of properties depending on the type of functionalization.[6] Fluorine as a substituent in particular has shown improved sorptive properties for specific guest molecules for gas-sensing and separation experiments.[7]

Upon closer inspection of fluorinated MOFs in particular, certain discrepancies of the resulting influence of the functionalization are revealed. FMOF-1, as reported by Yang *et al.*,[8] exhibits some impressive properties such as (super) hydrophobicity and a very high H_2-uptake (*e.g.*, 41 kg m^{-3} at 64 bar). Other reports on fluorinated systems however showed an insignificant influence of the H_2-uptake, when compared to an isostructural unfluorinated MOF.[9] Contrarily, they found a significant increase of the CO_2-uptake of the compound. It is thus apparent that the interactions of the internal MOF surface with specific guest molecules in question are of major importance to the properties found. Investigation of these interactions is not a trivial task. Guest molecules often only interact weakly with the host frameworks *via* non-covalent interactions, are mobile within the framework and the very frequently complex structure of the linker can make the interpretation of spectroscopic data, such as IR spectroscopy, difficult due to severe signal overlap. One of the most precise methods to observe molecular interactions is *via* single crystal X-ray diffraction (SCXRD). Some very successful examples of the analysis of guest molecules inside porous host materials *via* SCXRD have been shown by the group around M. Fujita, who later formalized their procedure as the crystalline sponge (CS) method.[10] In 2002, Fujita and co-workers published the synthesis and crystal structure of $\{[(ZnI_2)_3(tpt)_2]\cdot x(solvent)\}_n$ (tpt = 2,4,6-tris(4-pyridyl)triazine),[11] an interpenetrating coordination network, which is still regarded as the most potent crystalline sponge.[12] Part of the success as CS of this compound is attributed to its breathing behaviour.[12] Non-covalent interactions such as π–π-stacking can even be utilized to create functional porous environments, as was shown by the "cartridge" approach with the $\{[(ZnI_2)_3(tpt)_2]\cdot x(solvent)\}_n$ network.[13] In a recent review article, Fujita and others differentiate between robust MOFs and crystalline sponges

Department of Chemistry and Biochemistry, Institute for Inorganic and Materials Chemistry, University of Cologne, 50939 Cologne, Germany.
E-mail: uwe.ruschewitz@uni-koeln.de

† Electronic supplementary information (ESI) available: Detailed crystallographic data, additional views of the crystal structures, precession images, and selected difference Fourier maps. CCDC 2383895–2383900. For ESI and crystallographic data in CIF or other electronic format see DOI: https://doi.org/10.1039/d4ce01007h

via the response of the host material to the guest molecules.[12] Accordingly, crystalline sponges exhibit a form of guest recognition (*i.e.* breathing effects, formation of guest specific non-covalent interactions) that enables the crystallographic localisation of the guest molecules.

Recently, we have reported the synthesis, crystal structure and properties of a fluorinated MOF based on alkaline earth metal cations.[14] This compound, $[EA_5(3F\text{-}BTB)_3OAc(DMF)_5]$ (EA = Ca(II), Sr(II)), which was named UoC-9 (UoC: University of Cologne), consists of one-dimensional EA(II)O_x strands and a fluorinated derivative of the well-known BTB ligand (3F-BTB = 1,3,5-trifluoro-2,4,6-tris(4-carboxy-phenyl)benzene). The parallel strands are interconnected by the linkers forming a large void space (approx. 43–44% of the overall volume), accessible for solvent molecules, *i.e.* DMF (*N*,*N*-dimethylformamide) in this study, as was shown by SCXRD. A closer inspection revealed the unique host–guest interactions, the partially fluorinated linkers exhibit with the DMF guest molecules.[14] Part of the success of $\{[(ZnI_2)_3(tpt)_2]\cdot x(\text{solvent})\}_n$ by Fujita and co-workers has been attributed to the electron deficient tpt-linker, which preferentially stacks with electron richer π-systems of guest molecules.[12] This effect has also been observed in UoC-9, where the three fluorine substituents withdraw electron density from the central ring of 3F-BTB. This has led to the observation of amide-π-stacking inside the pores of UoC-9.[14] Another factor that Fujita and co-workers deem beneficial for the CS method is the interpenetrated nature of $\{[(ZnI_2)_3(tpt)_2]\cdot x(\text{solvent})\}_n$, where the individual frameworks can move with respect to each other, thus adapting the "optimized" pore size for the guest molecules.[12] In contrast, UoC-9 exhibits significant changes of its lattice depending on the guest loading as was shown by time-resolved PXRD experiments (PXRD: powder X-ray diffraction).[14]

Herein, we will present the refined X-ray single crystal structures of UoC-9(Ca) with six different guest molecules embedded in its pores. The CS method is well established to elucidate the structure of otherwise non-crystalline guest molecules[15] or to recognize different guest molecules.[12] In this work, we intend to utilize the CS behaviour to learn more about the interactions of solvent molecules and their functional groups with a MOF containing fluorinated linkers as well as to learn more about UoC-9 as a potential crystalline sponge, and how this behaviour influences properties like structural phase transitions.

Results and discussion

Single crystals of UoC-9(Ca) (UoC-9 hereon) were prepared by the methods described in our previous article.[14] The supernatant (a mixture of DMF and acetic acid) of these crystals was gradually exchanged with either acetylacetone (Hacac, b.p.: 140 °C, 54 electrons), *N*-methyl-2-pyrrolidone (NMP, b.p.: 202 °C, 54 electrons), benzonitrile (PhCN, b.p.: 188 °C, 54 electrons), toluene (PhMe, b.p.: 111 °C, 50 electrons), propylene carbonate (PC, b.p.: 242 °C, 54 electrons) or tetrahydrofuran (THF, b.p.: 66 °C, 40 electrons); for comparison: DMF, b.p.: 153 °C, 40 electrons. These solvents were chosen, as they are aprotic, since UoC-9 decomposes quickly in water, and as most of them show a comparatively low volatility in order to slow down the degradation of the single crystals by evaporation of the respective solvent. After the exchange of the supernatant (further details are given in the Experimental section), the colourless crystals remained intact and single crystal diffraction data was collected at 100 K. Due to the phase transition that as synthesized UoC-9 undergoes (and thus potential strain on the single crystals), the crystals mounted on the diffractometer were cooled down very slowly from RT to 100 K over several hours. The diffraction data revealed not only a significant effect of the guest molecules on the lattice parameters (Table 1), but also on the phase transition as observed for as synthesized UoC-9.

The structures presented herein were generally elucidated starting from the atom positions of the framework as previously published[14] and subsequent localization of the guest molecules by difference Fourier analysis. As the guest molecules often exhibit disorder, least square restraints were employed to retain sensible geometries of these molecules and the framework, where molecular fragments overlap. Thus, the individual bond lengths and angles will not be discussed in detail. Instead, we would like to focus the discussion on more general structural features, such as the distances between entire molecular fragments and lattice parameters, which can be determined reliably. Efforts were made to only model those guest positions, where the geometry of the guest was obvious from the difference Fourier map in order to prevent overfitting of the models. Any remaining electron density in the models was treated with the SQUEEZE[17] procedure within PLATON.[18] Since both *Ima*2 and $Pna2_1$ are acentric space groups and the models presented herein all contain unmodelled electron density, which would affect the Flack(*x*) parameter, they were generally refined as two component inversion twins. An increase of the unit cell volume is observed for all the herein presented guests. The crystals containing Hacac and PhCN as guests do not undergo a phase transition, which can easily be recognized from the missing reflections following the extinction conditions for body centred structures present in their diffraction patterns (Fig. S11 and S15, ESI†). The crystal containing NMP shows additional reflections indicating a tripling of the crystallographic *b*-axis (Fig. S16, ESI†). It was solved and refined as a superstructure in the space group $Pna2_1$ (*vide infra*).

Refinements of all crystal structures from these datasets, as expected, reveal an incorporation of the guest molecules into the pores of the framework. Comparing the expansion of the observed unit cell volumes (Table 1) with the respective sizes of the guests, a weak correlation might become apparent at first glance. However, in a second step, the

Table 1 Unit cell parameters obtained from X-ray single crystal diffraction data (Cu-Kα/Mo-Kα/synchrotron) in dependence of the embedded guest molecules. Additionally, the assigned space groups are given. All of the presented data was collected at 100 K. Additionally, the calculated molecular volume of the guests per molecule (V_{guest}),[16] the number of electrons found in the pores (s.a.v.) by the SQUEEZE procedure,[17] the estimated number of guest molecules per unit cell and their overall steric demand (SD_{guest}) are given

Guest	a [Å]	b [Å]	c [Å]	V [Å^3]	Space group	Guest volume per molecule[d] [Å^3]	Number of electrons in s.a.v. using SQUEEZE[c]	Estimated number of guest molecules/cell[e] (SD_{guest} [Å^3])
DMF[a]	31.6172(8)	16.5669(4)	28.5512(7)	14 955.1(6)	$Pna2_1$	116.2	254	54.4 (6321)
Hacac	31.5957(19)	16.8364(9)	28.2441(16)	15 024.7(15)	$Ima2$	148.4	2568	55.6 (8251)
THF	31.6409(19)	16.5291(9)	28.7463(15)	15 034.2(14)	$Pna2_1$	118.1	1777	56.2 (6637)
PhMe	31.7465(13)	16.6974(7)	28.4978(11)	15 106.2(11)	$Pna2_1$	143.8	1206	20 DMF + 25.9 PhMe (6048)
PC	31.6786(8)	16.5991(5)	28.8107(8)	15 149.7(7)	$Pna2_1$	125.7	1619	50.8 (6386)
PhCN	31.8875(14)	16.6009(7)	28.7479(11)	15 218.0(11)	$Ima2$	137.6	1423	20 DMF + 36.4 PhCN (7333)
NMP[b]	32.033(6)	16.553(3)[b]	28.956(6)	15 354(5)[b]	$Pna2_1$	148.8	1544[b]	51.7[b] (7687)

[a] Structural data as previously published.[14] [b] Solution of NMP@UoC-9 as 3*b* superstructure; all appropriate values in this table are divided by 3 for comparison with the other structures. [c] All electron density from not modelled solvent molecules removed by the SQUEEZE[17] program gives an estimate of the additional electrons/solvent molecules in the solvent accessible void (s.a.v.). [d] Calculated (V_{guest}) using volume increments as described by Koch and Fischer.[16] [e] Steric demand of the guest molecules per unit cell (SD_{guest}), calculated by the sum of all guest molecules multiplied with their calculated V_{guest} $\left(SD_{guest} = \sum_i V_{guest,i} \times n_{guest,i}\right)$.

amount of solvent molecules inside the pores also has to be taken into account. An, albeit crude, estimate of the amount of guest molecules inside the measured crystals can be obtained by the results of their treatment with the SQUEEZE program.[17] The values obtained, by adding the amount of the refined guest molecules (*vide infra*) to those estimated *via* the amount of additional electrons in the unit cell, are presented in Table 1. Considering these values clearly shows that the observed expansion of the unit cells is not dependent upon the sizes of the respective guests and the numbers of the embedded guest molecules, *i.e.* the calculated overall steric demand (SD_{guest}). Thus, finding the mechanisms of the response of UoC-9 to different guest molecules requires a closer look at the individual crystal structures. In the following, we will discuss the interplay of UoC-9 with the guest molecules along the factors shown in Scheme 1. These are comprised of the elongation of the SBU along the *a*-axis (c), the bulk steric demand of the guests as previously

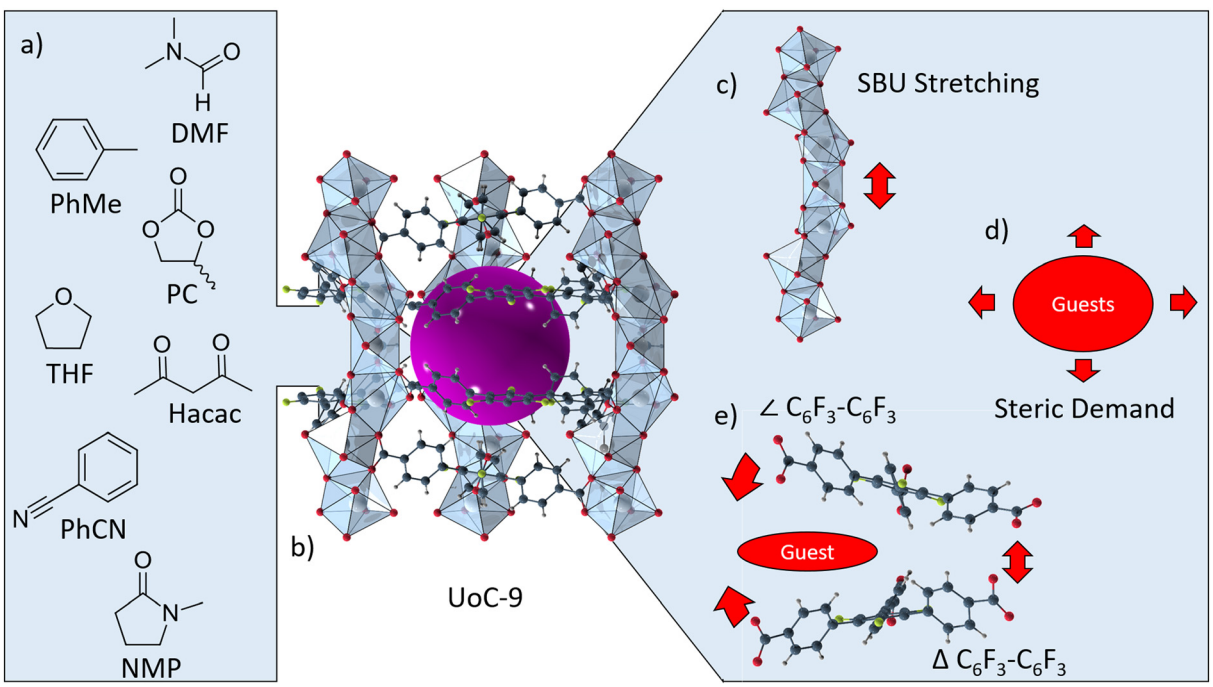

Scheme 1 Lewis structures of the guest molecules embedded in UoC-9 with their names as abbreviated in this work (a). Excerpt of the crystal structure of UoC-9 with one isolated pore, indicated by a purple sphere with a 5 Å radius (b). One isolated SBU of UoC-9 with an arrow indicating the stretching direction (c). Red ellipse with arrows symbolizing the general steric demand of the embedded guest molecules (d). Excerpt of the crystal structure of UoC-9 showing two 3F-BTB linker moieties involved in the intercalation of electron rich guest molecules in this MOF (e).

described (d) and the distances and angles between the 3F-BTB linkers that make up the C_6F_3 pocket after intercalation of guest molecules (e).

As there is an inherent dependency of the structure of UoC-9 on the presence of guest molecules (the framework was shown to collapse upon evaporation of DMF[14]), DMF@UoC-9 was chosen as the "neutral" framework to which these case studies will be compared to. In all cases except for PhMe and PhCN, the coordinating DMF molecules, present from the synthesis of UoC-9, are completely replaced by the added guest, facilitated by a large excess of the respective guest molecules in the equilibrium during the exchange procedure.

Hacac@UoC-9 remains in the body centred RT-modification at 100 K and exhibits an enlarged *b*-axis (by 1.62%) and a shortened *c*-axis (by 1.08%). The asymmetric unit features one Hacac molecule coordinated to Ca3, and disorder of one of the 3F-BTB linkers (Fig. S1, left, ESI†). The remaining two metal sites are saturated by oxygen atoms, most likely stemming from severely disordered Hacac molecules, which could not be modelled in a sensible way. A possible reason for the enlarged *b*-axis can be found in the disordered linker. The two positions of the linker are shifted by ~0.4 Å along the *b*-axis, in order to facilitate two different modes of coordination from one of the carboxylates to the Ca atoms (Fig. S1, left, ESI†). The involved benzoate moiety also twists significantly with an interplanar angle of 62° between the two positions. A further explanation for this particular behaviour is found when considering the contacts to the guest molecules. In DMF@UoC-9, this linker is involved in amide-π-stacking with DMF. This stacking seems to be absent in Hacac@UoC-9, which is emphasized by the absence of significant electron density in the difference Fourier map of the pocket between two linkers (Fig. S17, ESI†). This results in a decreased $C_6F_3\cdots C_6F_3$-ring distance of 5.7957(3)–6.4381(4) Å (measured from the centre points of the rings) compared to 6.5365(2) Å in DMF@UoC-9(LT) (Fig. S1, right, ESI†), which also explains the shortest observed *a*-axis among all guest@UoC-9 systems, even though Hacac is a considerably large guest. Considering that the largest steric demand (SD_{guest} = 8251 Å^3) by the guest molecules is calculated for Hacac@UoC-9 and the C_6F_3 pocket is unoccupied, the framework has to expand along the *b*-axis to increase the volume of the large pores (Scheme 1d). This is accompanied by a shrinkage of the *c*-axis (shortest observed among all compounds), which can be rationalized from the framework structure of UoC-9 (Fig. 1). Due to the interconnection of the CaO_x-strands by the 3F-BTB linkers, a motion, in which the strands drift further away from another along either the *b*- or *c*-axis, automatically pulls the strands along the respective other axis closer together. A satisfactory explanation, why Hacac as a guest specifically elongates the *b*-axis instead of the *c*-axis, which all other systems seem to prefer, cannot found within the structural data easily. It may be due to the (disordered) packing of Hacac inside the pores, which would exhibit a preference towards aligning the guest molecules along the *b*-axis.

The other system, where the room temperature modification of the framework is observed at 100 K, is PhCN@UoC-9. Therein, the DMF molecules coordinating to the SBU were not replaced by the PhCN guests, which instead occupy the s.a.v. of the MOF and the pocket, in which amide-π-stacking was observed for DMF in DMF@UoC-9. In the asymmetric unit, four different PhCN positions were refined, two of which are disordered and occupy the aforementioned pocket (Fig. S8, ESI†). In the context of protein structures, it was predicted that more electron deficient π-systems would interact with electron rich amides, forming energetically favoured stackings.[19] Accordingly, the electron rich cyanide moiety of one of the disordered PhCN molecules is inserted in-between the two C_6F_3 rings. This results in an increased distance between the two linkers (6.5502(3) Å), compared to the systems with an empty pocket (Fig. 2). Concomitantly, the *a*-axis is elongated by 0.85%, compared to DMF@UoC-9. The third largest steric demand of all systems was calculated

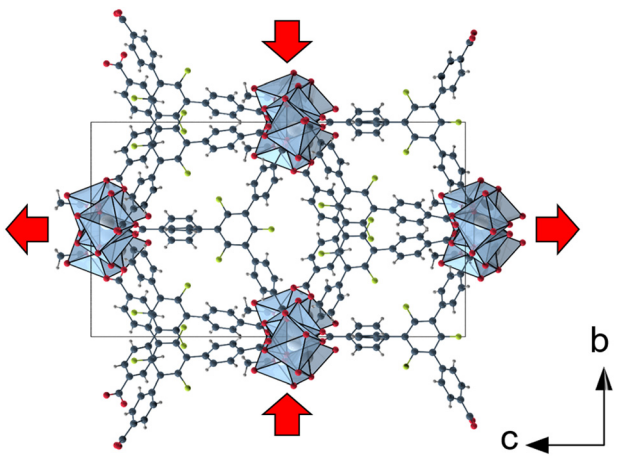

Fig. 1 Excerpt from the crystal structure of UoC-9 depicting one expanded unit cell with a view along the crystallographic *a*-axis. Arrows indicate the connected directions of expansion and contraction along the *b*- and *c*-axis.

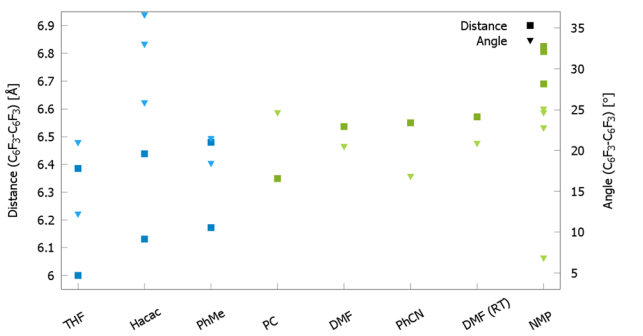

Fig. 2 Comparison of the $C_6F_3\cdots C_6F_3$ ring centre to ring centre distances (square) and interplanar angles (triangle) of the linkers in the different guest@UoC-9 systems. Symbols for systems with guest molecules encapsulated between two rings are marked in green and systems without guests in-between the rings in blue.

for PhCN (SD_{guest} = 7333 Å^3) with a considerable gap to the next lower entry. As Hacac@UoC-9 and PhCN@UoC-9 do not show a phase transition from *Ima*2 to *Pna*2$_1$ at lower temperatures, we thus propose that the bulk steric demand of the embedded guest molecules plays a crucial role for this phase transition.

In NMP@UoC-9 with the second highest steric demand of the guest, the space group *Pna*2$_1$ was observed at 100 K, which suggests a phase transition in this system. However, NMP@UoC-9 forms a superstructure with 3 × *b* (*vide infra*) so that the formation of a superstructure is obviously another way to accommodate larger guest molecule loadings (high SD_{guest}) without suppressing the phase transition. The remaining systems, which do undergo phase transitions as found in DMF@UoC-9, have estimated SD_{guest} values below 7000 Å^3 per unit cell.

In PhMe@UoC-9, the coordinating DMF molecules of the SBU are not exchanged, analogous to PhCN@UoC-9, and toluene molecules can only be refined within the pores of UoC-9. Two unique positions for toluene (PhMe) are found in the asymmetric unit and all five coordination sites for DMF can be refined as such (Fig. S6, ESI†). One of the three 3F-BTB linkers exhibits a similar disorder as was observed for Hacac@UoC-9 (largest shift along the *c*-axis by 0.5 Å), which is again accompanied by the absence of significant electron density within the $C_6F_3\cdots C_6F_3$ pocket. Analogously, the crystallographic *b*-axis is elongated by 0.8% (second largest reported herein). This suggests that the DMF molecules present after the synthesis have a structure directing effect, "binding" the two linkers involved in the pocket formation together by the formation of a sandwich complex. While it is surprising in the first instance that the electron rich π-system of PhMe does not intercalate between the linkers, this is reasonably explained by the larger steric demand of the phenyl unit. The pocket itself is surrounded by three non-coplanar benzoate moieties, which would collide with the hydrogen atoms of a hypothetically sandwiched toluene molecule. Instead, the guests interact with the phenylene moiety of an adjacent benzoate and coordinating DMF molecules, all of which are disordered over two positions. The occupancies of the toluene molecules were refined to 66.6% and 57.7%, respectively.

In THF@UoC-9, a similar disorder of the same 3F-BTB linker position in the asymmetric unit is observed. Again, the difference Fourier map indicates the $C_6F_3\cdots C_6F_3$ pocket to be empty (Fig. S18, ESI†), corroborating the structural impact of guest molecules in the $C_6F_3\cdots C_6F_3$ pockets. Appropriately, the shortest $C_6F_3\cdots C_6F_3$ distance is observed (Fig. 2). In this structure model, three THF positions were refined, all of which are coordinated to the SBU with one of them being disordered over two positions (Fig. S5, ESI†).

The PC@UoC-9 system is very similar to the DMF@UoC-9 system. It features five crystallographically unique positions for PC molecules, four of which are coordinated to the SBU and the remaining one occupies the $C_6F_3\cdots C_6F_3$ pocket. Two of these five positions are disordered in the presented model, attributable, in part, to the fact that the solvent used is a racemic mixture of the two enantiomers of PC (Fig. S7, ESI†). There is additional disorder of one of the benzoate moieties in the 3F-BTB linker, where the phenyl moieties are twisted by an interplanar angle of 38°. However, the attached carboxylate moieties are shifted only slightly from one another with no difference in their mode of coordination (Fig. S2, ESI†). The occupancy of the PC molecule inside the $C_6F_3\cdots C_6F_3$ pocket refines to a value close to one (therefore set to one in the presented structure) indicating an energetic preference of the intercalation of the electron rich carbonate. This is corroborated by the short $C_6F_3\cdots C_6F_3$ distance of 6.3491(2) Å found for PC@UoC-9 (Fig. 2) and serves to explain the comparatively short crystallographic *a*-axis found for this system (only 0.2% increase compared to DMF@UoC-9).

NMP@UoC-9 is a particularly interesting example due to its 3 × *b*-superstructure. The digitally generated precession images of the diffraction data recorded at a high intensity synchrotron facility clearly show a tripling of the *b*-axis (Fig. S16, ESI†). Since all atoms occupy the general Wyckoff position 4*a*, the asymmetric unit contains 3 × 5 = 15 Ca atoms, 3 × 3 = 9 3F-BTB linkers and 3 × 1 = 3 acetate anions only for the framework structure. NMP molecules replace DMF molecules coordinated to the Ca(II) strands and inside the pores such that twelve NMP molecules in the asymmetric unit coordinate to metal centres (five of them are disordered over two positions) and six were refined in the s.a.v. (Fig. S9, ESI†). The reason for the observed superstructure becomes apparent upon inspection of the SBU (Fig. 3).

In the NMP@UoC-9 system, two distinguishable CaO_x-strands are present (Ca1–Ca10 and Ca11–Ca15). They differ most significantly in the Ca1, Ca6 and Ca11 positions (cp. highlighted frame in Fig. 3), which are all equivalent in the DMF@UoC-9 (LT) structure. While Ca11 is similar to Ca1 in DMF@UoC-9, Ca1 in NMP@UoC-9 exhibits a different coordination sphere, accompanied by a

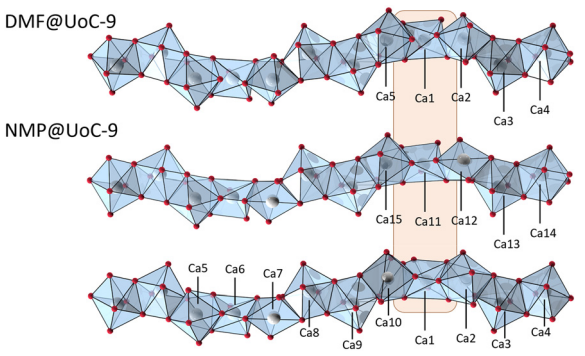

Fig. 3 Excerpts of the crystal structures of UoC-9(Ca) in its low temperature modification (top) and the NMP@UoC-9(Ca) system (bottom) showing CaO_x-strands with their coordination polyhedra with atom labels for the Ca-atoms inside one unit cell. The viewing direction is along the *c*-axis, the *b*-axis propagates from the bottom to the top of the figure. The frame is a guide for the eye (for details, see text).

shift away from Ca10 (cp. Ca1–Ca10$_{NMP@UoC-9}$ = 3.777(3) Å *vs.* Ca1–Ca5$_{DMF@UoC-9}$ = 3.6528(9) Å). Furthermore, the coordination sphere around Ca1 in NMP@UoC-9 is influenced by the disorder of one benzoate moiety (BTB_9: C30A–C36A and C30B–C36B). Instead of the bidentate coordination to Ca10 forming a μ_2-bridge to Ca1, which would be analogous to Ca5 in DMF@UoC-9, the carboxylate forms two single bonds to Ca1 and Ca10 (Fig. S3, ESI†). The latter case would naturally drive the Ca(II) cations further apart due to their repulsion, providing an explanation for the observation of the longest *a*-axis in the herein presented guest@UoC-9 systems. While this disorder is not unique for the presented guest@UoC-9 systems, the combination of one SBU (strand) with disorder and another one without is (Fig. S10, ESI†). To rationalize the guest molecules as the cause for this behaviour, it is necessary to analyse the $C_6F_3\cdots C_6F_3$ pockets in more detail. In NMP@UoC-9, the largest $C_6F_3\cdots C_6F_3$ ring distances are found ranging from 6.6897(13) Å to 6.8247(13) Å (Fig. 2). This can be explained by the larger steric demand of NMP compared to the other guests in this type of interaction, corroborated by the Hirshfeld surface analysis (*vide infra*). Thus, the appearance of the superstructure can be explained by the intercalation of a sterically more demanding guest between the 3F-BTB linkers of the pocket. The guest pushes them apart along the *a*-axis, elongating the unit cell in this direction, and rearranging the carboxylate units along the SBU. Comparing the bulk steric demand of the NMP guest to the aforementioned Hacac and PhCN systems, no phase transition would be expected. However, NMP@UoC-9 at 100 K may be understood as being a "halfway" point between the *Pna*2$_1$ and the *Ima*2 structure, where one of the disordered benzoate moieties in the asymmetric unit remains in its "RT *Ima*2 position" and the remaining ones shift to their "LT *Pna*2$_1$ conformations", which leads to the formation of the 3 × *b* superstructure.

An inspection of the Hirshfeld isosurfaces around the guest molecules intercalated in the $C_6F_3\cdots C_6F_3$ pockets reveals further interactions with the host framework. Fig. 4 shows the isosurfaces for PC@UoC-9 and PhCN@UoC-9 and the closest N–H and O–H contacts from the framework to the guest molecules. It can be seen that in both examples the electron rich functional groups form hydrogen bonds with the positively polarized hydrogen atoms of the outer benzoate moieties. This is corroborated by the sharp spikes in the delineated fingerprint plots corresponding to the Hirshfeld isosurfaces. The hydrogen atoms involved should be particularly polarized due to the strong electron withdrawing functional groups attached to the linker.[20] A similar behaviour is observed for NMP@UoC-9, where the same contacts between the oxygen atom of the guest to the arylic hydrogen atoms are formed (Fig. 5). This Hirshfeld isosurface further shows the contacts between the hydrogen atoms of the methylene group in α-position to the carbonyl function of

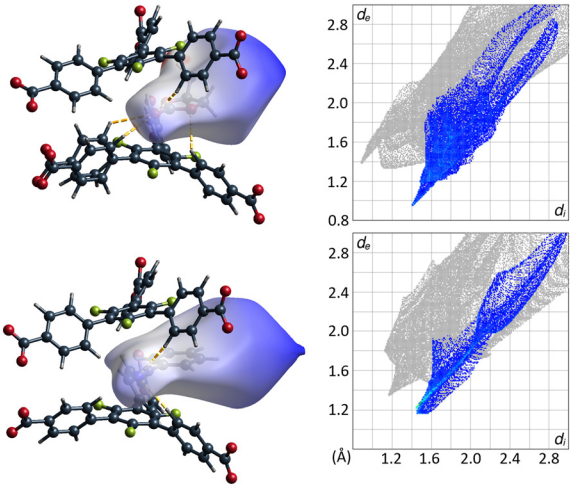

Fig. 4 PC (top) and PhCN (bottom) molecule shown with its calculated Hirshfeld isosurface (d_{norm}-mapping)[21] stacked between two 3F-BTB linkers in the framework of their respective guest@UoC-9 systems. Close contacts are highlighted with dashed orange lines. Fingerprint plots of the respective Hirshfeld isosurfaces (displayed to the right) show the contacts from inner O/N atoms to outer H atoms contributing to 20.8% and 13.2% of the surface areas, respectively.

the guest to the carbon atoms of the C_6F_3-rings, which are shorter than the sum of the respective vdW-radii. These contacts, which are assumed to contribute to a repulsion of the involved fragments, nicely explain, why the largest $C_6F_3\cdots C_6F_3$ distance is observed for this system. The examples presented herein show clearly that the $C_6F_3\cdots C_6F_3$ pocket is very selective towards electron rich guests – or fragments thereof – smaller than a phenyl ring. At this point it is somewhat surprising that the $C_6F_3\cdots C_6F_3$ distances seem to respond as expected to the insertion of guest molecules, while the involved angles do not follow a clear trend, as their

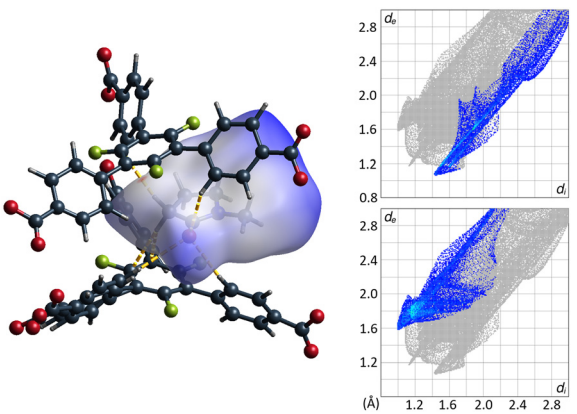

Fig. 5 NMP molecule shown with its calculated Hirshfeld isosurface (d_{norm}-mapping)[21] stacked between two 3F-BTB linkers in the framework of the NMP@UoC-9 system. Close contacts are highlighted with dashed orange lines. Fingerprint plots of the respective Hirshfeld isosurface (displayed to the right) show the contacts from inner O/H atoms to outer H/C atoms contributing to 14.5% and 19.5% of the surface area, respectively.

spread shown in Fig. 2 does not allow to recognize any correlation.

The guest@UoC-9 system is, due to its sensitivity to water and degradation upon evaporation of the guest molecules, not as suitable to be used for the CS method as *e.g.* $\{[(ZnI_2)_3(tpt)_2]\cdot x(solvent)\}_n$.[12] Furthermore, UoC-9 is significantly less flexible than other crystalline sponges. However, it does exhibit promising behaviour for chemical sensing of the herein described guests *via* the $C_6F_3\cdots C_6F_3$ pockets, which could be tailored into other, eventually more stable porous frameworks.

Experimental

Synthetic procedures

UoC-9(Ca). 10.0 mg of H_3-3F-BTB (synthesized by the procedure published by Christoffels *et al.*[22]) (0.02 mmol) and 30.0 mg $Ca(NO_3)_2\cdot 4H_2O$ (0.13 mmol) were dissolved in a mixture of 4 mL DMF and 0.2 mL acetic acid. The mixture was heated for 48 h at 100 °C yielding colourless crystals of sufficient size for SCXRD.

Guest exchange. Suitable crystals of UoC-9(Ca) were transferred to a screw cap vial *via* a pipette with the supernatant. Selected solvents/guests were added to the suspension, before the excess liquid was removed again *via* a pipette (crystals always remained under a minimal layer of liquid). This step was repeated (3–4 times), until complete exchange of the supernatant was assumed and finally proven by SCXRD. The crystals remained in the liquid for at least 72 h, before they were selected under a microscope and immediately mounted under a cooled N_2 stream on the diffractometer.

Analytical methods

Single crystal X-ray diffraction (SCXRD). Single crystal diffraction data was collected on a Bruker APEX-II CCD diffractometer (Cu-Kα radiation, mirror-monochromator, λ = 1.54187 Å), on a Bruker D8 venture diffractometer (Mo-Kα radiation, mirror-monochromator, λ = 0.71075 Å) or on the Kappa diffractometer of the P24.1 beamline of the PETRA III facility at the Deutsches Elektronen-Synchrotron (DESY) (λ = 0.50000 Å), Hamburg/Germany. Suitable crystals were selected under a microscope and quickly mounted under a cooled N_2 stream on the diffractometer, as the crystals loose their guest molecules very easily. The temperature was controlled with an Oxford Cryostream 800 system. The exact cooling rates for the individual measurements varied, but were kept below 1 K min^{-1}. The data reduction and correction for absorption was carried out using SAINT[23] and SADABS[24] inside the APEX5 (ref. 25) program package for the diffraction data collected in house. Data collected at the DESY was reduced and corrected inside the CrysAlisPro 1.171.41.112a program package.[26] Initial models, unless otherwise stated, were obtained with SHELXT[27] and were subsequently refined using SHELXL.[28] The difference Fourier maps were calculated using SHELXL[28] and visualized in ShelXle[29] and VESTA.[30]

Hirshfeld-surface analysis. To calculate the Hirshfeld surfaces, the CrystalExplorer 21.2 (ref. 31) program-package was used. All hydrogen bond lengths were set to normalized values (1.083 Å for C–H) by the program prior to the calculation. The electron densities for each atom type were taken from the basis sets calculated by Koga *et al.*[32] and the surfaces were generated on the very high setting for the number of grid points.

Conclusions

In conclusion, we have shown the successful embedment of six different guest molecules inside the fluorinated framework of UoC-9(Ca) *via* liquid exchange. The guest molecules are common solvents with different functional groups and polarities and were all confirmed to reside inside the framework by the elucidation of single crystal diffraction data from the exchanged guest@UoC-9 systems. Of these six guest@UoC-9 systems, those with encapsulated Hacac and PhCN do not undergo a phase transition from *Ima*2 to $Pna2_1$ down to 100 K that was observed for the as-synthesized UoC-9 (containing DMF), which is attributed to the larger bulk steric demand of these guest molecules (Hacac, PhCN). NMP@UoC-9 exhibits a 3 × *b* superstructure representing an "intermediate" phase between the RT modification (*Ima*2, Z = 4) and the low temperature modification ($Pna2_1$, Z = 4) of UoC-9(Ca). Throughout the detailed analysis of the guest@UoC-9 systems, it became clear that guest molecules with different functionalities affect the lattice of UoC-9 in different ways, which is summarized in Table 2.

Whereas the bulk steric demand of the guest molecules is mostly reflected in the occurrence/absence of the phase

Table 2 Comparison of the calculated molecular volumes of single guest molecules (V_{guest}) and the overall steric demand (SD_{guest}) with some structural properties of the different guest@UoC-9 systems discussed in this work (for details, see Table 1)

Guest	V_{guest} [Å]	SD_{guest} [Å^3]	Phase transition?	a/a_{DMF}	b/b_{DMF}	c/c_{DMF}	$C_6F_3\cdots C_6F_3$ pocket filled?
Hacac	148.4	8251	No	0.999	**1.016**	**0.989**	No
PhCN	137.6	7333	No	1.009	1.002	1.007	Yes
NMP	148.8	7687	3 × *b* supercell	**1.013**	0.999	**1.014**	Yes
DMF	116.2	6321	Yes	1	1	1	Yes
THF	118.1	6637	Yes	1.001	0.998	1.007	No
PhMe	143.8	6048	Yes	1.004	1.008	0.998	No
PC	125.7	6386	Yes	1.002	1.002	1.009	Yes

transition or an increase/shrinkage of the *b*- and *c*-axes, stacking interactions within the $C_6F_3\cdots C_6F_3$ pocket cause an elongation of the *a*-axis. The bulk steric demand of the guests is not well reflected in the unit cell volume due to their different locations in the MOF (large pore *vs.* $C_6F_3\cdots C_6F_3$ pocket) and interactions of the guest molecules with the framework. In our ongoing work, we aim to further improve our understanding of interactions in fluorinated host–guest systems. This is of particular importance for both the crystallization and thus synthesis of these systems as well as their material properties, *e.g.* adsorption of gases.

Data availability

The data that support the findings of this study are available in the ESI† of this article. Deposition number(s) 2383895 (for Hacac@UoC-9), 2383896 (for THF@UoC-9), 2383897 (for PhMe@UoC-9), 2383898 (for PC@UoC-9), 2383899 (for PhCN@UoC-9), and 2383900 (for NMP@UoC-9) contain the ESI† crystallographic data for this paper. These data are provided free of charge by the joint Cambridge Crystallographic Data Centre and Fachinformationszentrum Karlsruhe Access Structures service.

Author contributions

S. S. S. elucidated all of the herein reported crystal structures, carried out the guest exchange procedure for NMP@UoC-9 and PhCN@UoC-9, supervised F. P. D. during his work and wrote the first draft of the original manuscript. F. P. D. carried out the guest exchange procedures for all remaining guests. U. R. supervised S. S. S. and F. P. D. during their work and wrote parts of the original manuscript. All authors reviewed and approved the final form of the submitted manuscript.

Conflicts of interest

There are no conflicts to declare.

Acknowledgements

We would like to thank Carsten Paulmann for his help with the SCXRD measurements at the DESY in Hamburg, Jörg Neudörfl and Silke Kremer with the in-house SCXRD measurements and the German Science Foundation (DFG) for financial support (Project No. RU 546/12-1).

Notes and references

1 O. M. Yaghi, G. Li and H. Li, *Nature*, 1995, **378**, 703–706.
2 A. U. Czaja, N. Trukhan and U. Müller, *Chem. Soc. Rev.*, 2009, **38**, 1284–1293.
3 H. Furukawa, K. E. Cordova, M. O'Keeffe and O. M. Yaghi, *Science*, 2013, **341**, 1230444, (12 pages).
4 R. Freund, O. Zaremba, G. Arnauts, R. Ameloot, G. Skorupskii, M. Dincă, A. Bavykina, J. Gascon, A. Ejsmont, J. Goscianska, M. Kalmutzki, U. Lächelt, E. Ploetz, C. S. Diercks and S. Wuttke, *Angew. Chem., Int. Ed.*, 2021, **60**, 23975–24001.
5 J. Hao, X. Xu, H. Fei, L. Li and B. Yan, *Adv. Mater.*, 2018, **30**, 1705634, (22 pages).
6 Y. Lin, C. Kong and L. Chen, *RSC Adv.*, 2016, **6**, 32598–32614.
7 A. Ebadi Amooghin, H. Sanaeepur, R. Luque, H. Garcia and B. Chen, *Chem. Soc. Rev.*, 2022, **51**, 7427–7508.
8 C. Yang, X. Wang and M. A. Omary, *J. Am. Chem. Soc.*, 2007, **129**, 15454–15455.
9 K. Peikert, F. Hoffmann and M. Fröba, *CrystEngComm*, 2015, **17**, 353–360.
10 Y. Inokuma, S. Yoshioka, J. Ariyoshi, T. Arai, Y. Hitora, K. Takada, S. Matsunaga, K. Rissanen and M. Fujita, *Nature*, 2013, **495**, 461–466.
11 K. Biradha and M. Fujita, *Angew. Chem., Int. Ed.*, 2002, **41**, 3392–3395.
12 N. Zigon, V. Duplan, N. Wada and M. Fujita, *Angew. Chem., Int. Ed.*, 2021, **60**, 25204–25222.
13 M. Kawano, T. Kawamichi, T. Haneda, T. Kojima and M. Fujita, *J. Am. Chem. Soc.*, 2007, **129**, 15418–15419.
14 S. S. Sebastian, F. P. Dicke and U. Ruschewitz, *Dalton Trans.*, 2023, **52**, 5926–5934.
15 N. Wada, R. D. Kersten, T. Iwai, S. Lee, F. Sakurai, T. Kikuchi, D. Fujita, M. Fujita and J. K. Weng, *Angew. Chem., Int. Ed.*, 2018, **57**, 3671–3675.
16 E. Koch and W. Fischer, *Z. Kristallogr.*, 1980, **153**, 255–263.
17 A. L. Spek, *Acta Crystallogr., Sect. C: Struct. Chem.*, 2015, **71**, 9–18.
18 A. L. Spek, *J. Appl. Crystallogr.*, 2003, **36**, 7–13.
19 M. Harder, B. Kuhn and F. Diederich, *ChemMedChem*, 2013, **8**, 397–404.
20 G. S. Remya and C. H. Suresh, *Phys. Chem. Chem. Phys.*, 2016, **18**, 20615–20626.
21 M. A. Spackman and D. Jayatilaka, *CrystEngComm*, 2009, **11**, 19–32.
22 R. Christoffels, C. Breitenbach, J. P. Weber, L. Körtgen, C. Tobeck, M. Wilhelm, S. Mathur, J. M. Neudörfl, M. S. Z. Farid, M. Maslo, E. Strub and U. Ruschewitz, *Cryst. Growth Des.*, 2022, **22**, 681–692.
23 *SAINT*, Bruker AXS Inc., Madison, Wisconsin, USA, 2012.
24 *SADABS*, Bruker AXS Inc., Madison, Wisconsin, USA, 2001.
25 *APEX5*, Bruker AXS Inc., Madison, Wisconsin, USA, 2023.
26 *CrysAlis PRO*, Agilent Technologies Ltd, Yarnton, Oxfordshire, England, 2021.
27 G. M. Sheldrick, *Acta Crystallogr., Sect. A: Found. Adv.*, 2015, **71**, 3–8.
28 G. M. Sheldrick, *Acta Crystallogr., Sect. C: Struct. Chem.*, 2015, **71**, 3–8.
29 C. B. Hübschle, G. M. Sheldrick and B. Dittrich, *J. Appl. Crystallogr.*, 2011, **44**, 1281–1284.
30 K. Momma and F. Izumi, *J. Appl. Crystallogr.*, 2008, **41**, 653–658.
31 P. R. Spackman, M. J. Turner, J. J. McKinnon, S. K. Wolff, D. J. Grimwood, D. Jayatilaka and M. A. Spackman, *J. Appl. Crystallogr.*, 2021, **54**, 1006–1011.
32 T. Koga, K. Kanayama, T. Watanabe, T. Imai and A. J. Thakkar, *Theor. Chem. Acc.*, 2000, **104**, 411–413.

